Optical Engineering

OpticalEngineering.SPIEDigitalLibrary.org

Progress and opportunities in the development of nonmechanical beam steering for electro-optical systems

Paul F. McManamon
Abtin Ataei

SPIE.

Paul F. McManamon, Abtin Ataei, "Progress and opportunities in the development of nonmechanical beam steering for electro-optical systems," *Opt. Eng.* **58**(12), 120901 (2019), doi: 10.1117/1.OE.58.12.120901.

Optical Engineering 58(12), 120901 (December 2019)

REVIEW

Progress and opportunities in the development of nonmechanical beam steering for electro-optical systems

Paul F. McManamon* **and Abtin Ataei**
Exciting Technology LLC, Dayton, Ohio, United States

Abstract. We discuss over three decades of progress in nonmechanical beam steering, provide a comparison of approaches being developed, and comment on promising approaches not yet fully developed. Most of the work in nonmechanical beam steering has been for narrowband optical systems, but a brief discussion is provided of broadband. The majority of the nonmechanical approaches to beam steering create a tilted optical path delay (OPD) to change the wavefront, but some directly create a phase delay. OPD-based approaches may be true time delay, with no resets or modulo $2\pi n$ optical phased arrays that have resets. Most of the nonmechanical optical beam steering approaches tilt an existing wavefront and are called space fed approaches, because the beam is already formed when the wavefront is tilted. For the majority of radar nonmechanical beam steering, the tilted wavefront is formed by individual transmit/receive modules. Periodic structures (gratings) spread different wavelengths of light in angle, thus steering light, and are also used for nonmechanical steering. Our paper is derived from a conference paper presented at Photonics West in February 2019. [DOI: 10.1117/1.OE.58.12.120901]

Keywords: optical phased array; nonmechanical beam steering; mechanical beam steering; optical apertures.

Paper 190080V received Jan. 26, 2019; accepted for publication Nov. 27, 2019; published online Dec. 24, 2019.

1 Introduction

This paper explores the history of the development of electro-optical nonmechanical beam steering since 1985.[1] Most of the paper discusses nonmechanical beam steering for narrow band systems. The authors include broadband nonmechanical beam steering, even though progress in nonmechanical broadband optical beam steering has been limited.

The most common way to build optical phased arrays (OPAs) is by dynamically creating an optical path delay (OPD). A second way is to create a phase difference. For the design wavelength, there will be a substantial equivalence between OPD and phase-based approaches, but the fundamental method of delaying light will be different. Most OPA systems are based on creating an OPD. The phase-based approach is based on the work of Pancharatnam in his classic 1955 paper.[2] Both techniques will be discussed, and specific OPAs will be categorized as one, or the other, beam steering approach. Phase delay-based approaches are very thin, similar to modulo $2\pi n$-based OPAs, which will be discussed soon, but do not require resets, because phase is the same for 0 or any multiple of 2π phase. Phase automatically returns to zero each time 2π phase is completed. Both modulo $2\pi n$ OPD-based beam steering and the phased-based approach use periodic structures. These are gratings. Any grating will steer light of different wavelengths to different angular locations based on how light of different wavelengths interfere to create maximas and minimas. A simple grating will disperse wavelengths in an angle, providing a method of nonmechanical beam steering if the practitioner can change the wavelength of light.

OPD-based beam steering will be discussed first. The OPD-based approach is further subdivided into true time delay and modulo 2π-based time delay. The modulo 2π-based OPD approach allows use of a much thinner active medium than true time delay but requires OPD resets, which cause dispersion, making the OPA narrow band unless something is done eliminate this dispersion. True time delay OPA approaches are broadband but require a much larger OPD if a moderate or larger aperture is steered to a moderate or large angle.

A second way to divide nonmechanical steering is between steering an already formed beam, or steering a beam as it is formed. Most optical nonmechanical optical beam steering steer an already formed beam, which is called space fed beam steering. Most radar-based phased arrays steer a beam as it is formed, using individual transmit receive T/R modules. Some chip scale modulo $2\pi n$-based OPAs are being worked under various programs, but the technology is immature.

All gratings are dispersive, no matter if they are reflective or transmissive, or phase or amplitude. Gratings act as point scatterers, and different wavelengths will have constructive inference at different angles, where the path to a given spot from multiple scatterers is a multiple of the specific wavelength.

2 Optical Path Delay-Based OPAs

2.1 *Modulo $2\pi n$ Space-Fed Beam Steering Approaches*

The Modulo $2\pi n$ beam steering approach is based on using a thin, dynamic, OPD to do beam steering. For a narrow

*Address all correspondence to Paul F. McManamon, E-mail: paul@excitingtechnology.com

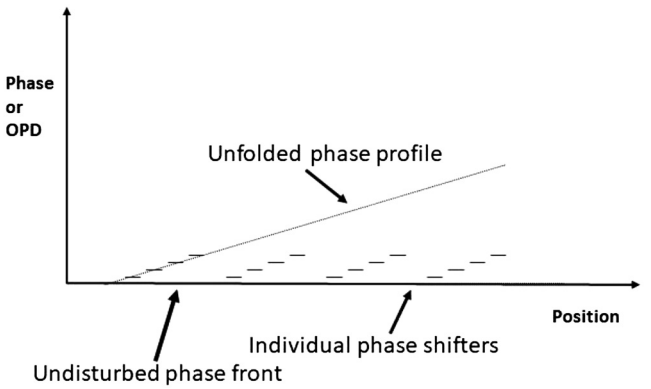

Fig. 1 Modulo 2π phase shifting to create beam steering.

wavelength, it is possible to take advantage of the fact that light is a sine wave. With sine waves, it does not matter if there is 0, 2π, 4π, or $2\pi n$ phase shift. For the design wavelength, the OPDs of any integer multiplied by wavelength ($n\lambda$) will be the same phase. Therefore, as one moves across the width of the imaginary prism (shown in Fig. 1), one can subtract $2\pi n$ of phase every time the phase reaches $2\pi n$. This results in a sawtooth OPD profile, and a phase profile that would result from propagation through a full prism and steers light in the same manner as a prism would. Because a reset occurs every time, the OPD reaches $2\pi n$, smaller angles have a larger lateral distance between resets. This is called variable pitch modulo 2π beam steering.[3]

As seen in Fig. 1, for variable pitch beam steering, when the OPD reaches a multiple of one wavelength (λ), a reset occurs, because an OPD of zero and a multiple of one wavelength would be the same phase. It should be noted that while resets must be multiples of a single wavelength, they can be initiated at OPDs, which are not an exact multiple of one wavelength. This provides design flexibility to provide very accurate pointing, to improve speed, and provide other design opportunities.[4,5] For example, a one-λ reset can occur after reaching an OPD of 1.1λ.

The benefit of using a modulo $2\pi n$ phase profile is that the required OPD can be small, allowing it to be written dynamically. The minimum required OPD is approximately equal to the wavelength of the light being steered. If, for example, there are 10 steps to reach 360 degrees of phase shift, only 324 deg or 9 steps will be needed. The 10th step would be 360 deg but is instead 0 deg, which is the same phase as 360 deg.

The modulo $2\pi n$ steering approach, however, makes the beam steerer very wavelength-dependent (dispersive).[6,7] The largest angle one can steer to, using the modulo 2π approach, is determined by the size of the smallest reset distance possible for the desired steering efficiency. Because a reset subtracts one, or a multiple of one, design wavelength, the sine of the steering angle is the wavelength divided by the reset distance:

$$\sin(\theta) = \lambda/\Lambda, \tag{1}$$

where θ is the steering angle, λ is the wavelength, and Λ is the lateral reset distance.

According to Eq. (1), as the lateral reset distance gets smaller, the angle gets larger. The size of a reset remains $n\lambda$. This means that the largest angle for a given wavelength is determined by the smallest possible lateral reset distance. This discussion is for variable period modulo $2\pi n$ beam steering.

For a circular aperture, the Fraunhofer diffraction pattern provides an intensity distribution that is the Airy pattern.[8] Although much of the electro-optics (EO) community use the angular distance from the middle of the beam to the zero point as a beam width metric, the authors prefer to use the radar convention, of the angular full-width half-maximum (FWHM) beam divergence as an appropriate beam width metric. For the Airy pattern, one can calculate that the FWHM beam width is

$$\theta \cong 1.03\frac{\lambda}{D}, \tag{2}$$

where θ is beam divergence, λ is the wavelength of the electromagnetic radiation, and d is the width of the individual radiator. The authors usually set the factor of 1.03 to 1, as a reasonable approximation. For a Hamming window function, the factor in Eq. (2) is 1.055.[9] Radar engineers often use the Hamming window function for a beam to reduce sidelobes. Skolnik, a classic radar textbook, describes values appropriate for different antenna beam patterns in Table 7.1 of his classic textbook.[10]

If the phase can be matched among many individual radiators, the beam will become narrower in angle proportional to the increase in the effective size of the radiator. If the full array is uniformly illuminated, then it is possible to substitute into Eq. (2) as follows:

$$D = nd, \tag{3}$$

where n is the number of individual radiators assembled to make the large radiator, and where it is assumed that the pitch of the radiator separations is equal to the width of the radiator (i.e., unity fill factor). For Gaussian illumination of the full array, compared to uniform illumination, the effective size of the large aperture is reduced and the beam divergence increases. The allowed amount of clipping of the Gaussian beam by the aperture array determines how much the effective aperture size is reduced. By adjusting the phasing among the individual elements, the narrow beam can be steered under the envelope of the larger beam resulting from an individual radiator.

Phased array microwave radars steer the beam to angles >45 deg. To do this, the radars use individual radiators that are at a half-wavelength spacing or closer. In radar, the conventional discussion of half-wavelength spacing says individual phase-adjustable radiators must be no larger than half wavelength to reduce grating lobes.[11] This is a different view of the same physics. From Eq. (2), if D equals one half of λ, then $\theta = 2.06$ radians or 118 deg. This is the full-beam width at the half-power points. Plus or minus 45 deg would be a 90-deg full width in angle, so it is possible to steer plus or minus 45 deg and still be significantly above the half-power point, neglecting the cosine factor loss in the projected area of the aperture.

One of the main efficiency considerations is the flyback region, which occurs at a reset. The size of the flyback region may be determined by fringing fields.[12] This effect is a result of the inability of the device to change its electric field profile

instantaneously in space. The flyback region substantially reduces the fill factor of the grating because light hitting the device in the flyback region will be deflected in the wrong direction. The flyback region depends primarily on the structure of the modulo 2π beam steering device. Active EO materials, such as liquid crystals (LCs) also have limitations on how quickly the index can change in space, which can act similar to fringing fields in limiting steering efficiency by causing a region that steers the wrong direction, when the OPD is reduced by an amount that will cause modulo $2\pi n$ reduction in phase (a reset).

The reset period Λ can consist of q electrodes of size w, each separated by the spacing of s. Therefore, the deflection angle will depend on the number of electrodes in each reset, the size of each electrode and the spacing between the electrodes, allowing Eq. (1) to be rewritten as follows:

$$\sin\theta = \frac{\lambda}{q(w+s)}, \tag{4}$$

where w is the width of an electrode, s is the spacing between electrodes, and q is the number of electrodes. The active layer thickness should be made as thin as possible to minimize the flyback region. The electrode size, spacing, and the number of electrodes in each reset should be optimized to not only satisfy the desired deflection angle in Eq. (4) but also to maximize efficiency. The number of electrodes in each reset also imposes another effect called quantization effect, which will be explained later in this paper.

Equation (5) gives the approximated efficiency of LC-based beam scanner due to flyback region effects:

$$\eta_f = \left(1 - \frac{\Lambda_F}{\Lambda}\right)^2, \tag{5}$$

where η_f is efficiency due to the fringing field, Λ_F is the width of the flyback region, and Λ is the width between resets.[13]

Figure 2 shows that during the flyback portion of the phase profile, the beam is deflected in the wrong direction. Fringing fields make it impossible to impose an electric field that stays only between the small electrodes. Instead, the field expands outward to each side of the small electrode. As a rule of thumb, the narrowest width of a voltage region above an electrode is about the thickness of the layer between the electrode and the ground plane.[14] Since the thickness of the active media layer is often larger than the spacing between the electrodes, it can be seen that fringing fields can cause a significant loss in efficiency. For transmissive beam steering, the cell has to be about as thick as

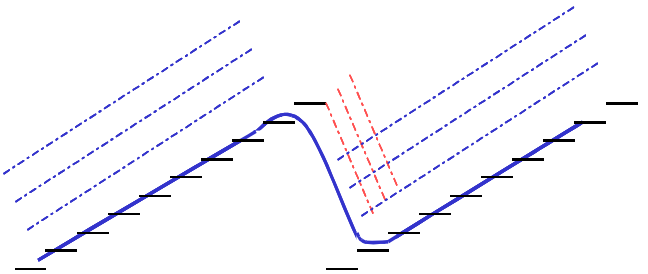

Fig. 2 The effect of fringing fields on phase profile.

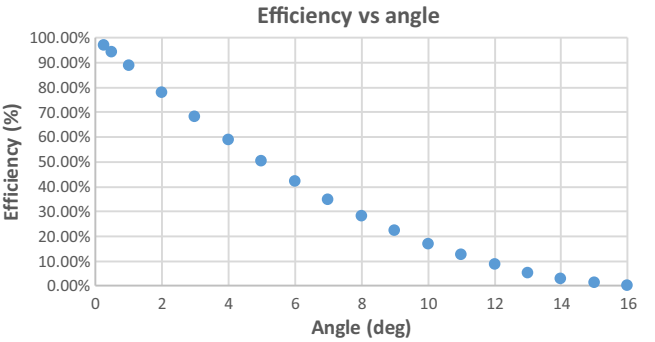

Fig. 3 Efficiency versus deflection angle limited by fringing fields effects for a conventional LC-based beam steering.

required to obtain one wavelength, or 2π phase, of OPD. With a birefringence of 0.3, this means the cell has to be about 3.3 times one wavelength in thickness. According to Eqs. (4) and (5), which give the deflection angle and efficiency, Fig. 3 shows how fast the efficiency drops as a function of deflection angle for a conventional LC-based thin-film scanner, assume a 0.3 birefringence, and a wavelength of 1.55 μm. Therefore, for high efficiency, it is necessary to limit the steering angles used for saw-tooth phase profile LC continuous steering to very small angles—on the order of a degree. For a quarter of a degree of angular steering, the steering efficiency is 98%. For 1-deg steering, it is down to ~90% efficiency. For 1-deg steering in both azimuth and elevation, the loss needs to be squared, so it would be about ~80% steering efficiency. This is a significant limitation for use as the fine angle steering before a wide-angle coarse steering element.

The second contribution to steering efficiency is from the discrete nature of the phase steps. Equation (6) gives the loss in efficiency from using discrete steps:

$$\eta_q = \left[\frac{\sin(\pi/q)}{\pi/q}\right]^2, \tag{6}$$

where η_q is the efficiency due to the quantization issue, and q is the number of steps in a reset period ramp.[15]

Table 1 and Fig. 4 show the efficiency versus number of steps in a ramp. Some early LC beam-steering work avoided the loss associated with discrete steps, discussed above, using two electrodes and a continuous ramp of voltages.[15] In this approach, a linear ramp in electric field was used instead of discrete phase steps. Initially, it was not obvious which approach would be preferred, but at the time the discrete steps did not provide a significant loss, and the linear region of the voltage versus phase shift was only a small portion of the full phase shift available from an LC cell, so it was necessary to make the LC cell thicker.

The significant loss using LC beam deflection had to do with fringing fields.[6] This loss was not affected using discrete steps versus a linear profile. The net result is the linear LC phase ramp approach to steering optical beams was not pursued further at that time. If a different active material is used, this approach could become attractive. Fringing fields are the main issue to address to increase the efficiency of modulo $2\pi n$ beam steering. This is being addressed and can result in steering efficiently to larger angles.[16] Figure 5 shows steering to 3 deg with 91% efficiency using fringing field

Table 1 Steering efficiency limited by the digitization.

q	Efficiency
1	0.0
2	40.5
3	68.4
4	81.1
5	87.5
6	91.2
7	93.5
8	95.0
9	96.0
10	96.8
12	97.7
14	98.3
16	98.7
18	99.0
20	99.2

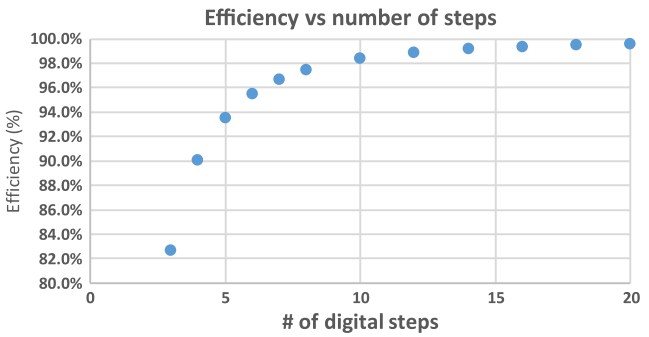

Fig. 4 Steering efficiency limited by the digitization.

mitigation techniques but being limited by the LCs resistance to fast spatial change.

2.1.1 *LC modulo 2π OPAs*

The initial OPA work implemented in the 1980s was modulo $2\pi n$ beam steering using LCs. Initially, the fringing field effects were not well understood, so Raytheon made a 4-cm-wide OPA on 1-μm pitch, with 40,000 phase shifters, shown in Fig. 6(a). By contrast, the microwave Pave Paws radar, shown in Fig. 6(b), has 7000 phase shifters. This gives an idea of the difference in scale of radio frequency (RF) versus optical phased arrays. Since the frequency of Pave Paws search radar is low, its phase shifters are significantly larger than an X-band radar. The Pave Paws AN/FPS-115 radar consists of two phased arrays of antenna elements, mounted on two sloping sides of the 105-foot high-transmitter building, which are oriented 120 deg apart in azimuths. The radar

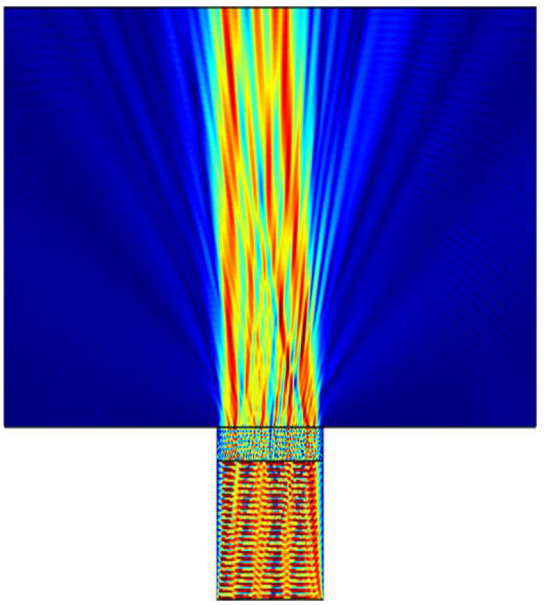

Fig. 5 91% steering efficiency at 3 deg, using LCs with 0.3 birefringence.

operates in the ultra-high frequency band, between 420 and 450 MHz, and has a wavelength between 71 and 67 cm.[17]

In the 1990s, a small business, Boulder Nonlinear Systems (BNS), also started to make LC OPAs. The first commercial OPA was produced by BNS in 1999. It is a 1×4096 OPA, on 1.8-μm pixel pitch. The device is 0.74 cm $\times$ 0.74 cm. Then BNS developed a larger OPA, which became available in 2003. It is $1 \times 12{,}228$ on a 1.6-μm pitch. It took up to 13.2 V to address it and was 19.2×19.2 mm in size. One of the reasons the OPA development was started with LCs is the large birefringence possible, and the low voltage required to impose that birefringence. To develop these OPAs, BNS leveraged the work that had been done previously with LC on silicon displays.[18]

Nematic LCs are relatively slow to respond, on the order of 10 ms. The speed of a nematic LC is proportional to one over the square of the thickness layer. This means longer-wavelength LC beam steerers can be significantly slower than shorter-wavelength beam steerers since using modulo $2\pi n$ beam steering requires a layer thickness related to the wavelength of the light being steered. The turn-on time of nematic LC can be improved by increasing voltage, but for a nematic LC, the turn-off time remains the same, unless a dual-frequency LC is used.[8] A dual-frequency LC drives the LC on at one frequency and off at a different frequency. With a dual-frequency LC, both the turn-on time and turn-off times can be improved using a higher voltage, but the drive electronics are more complicated, and dual-frequency LCs are more temperature sensitive. Depending on the dual-frequency LC material used, the two frequencies might be 1 and 50 kHz, as representative values. Although some researchers pursued dual-frequency LCs, they never became prevalent because of the limitations stated above.

One approach to increasing the switching speed of nematic LC beam steering devices that gained interest was polymer network LCs. A polymer is mixed with the LC to effectively make many thin cells. This requires a higher drive voltage and has an effectively lower birefringence, because

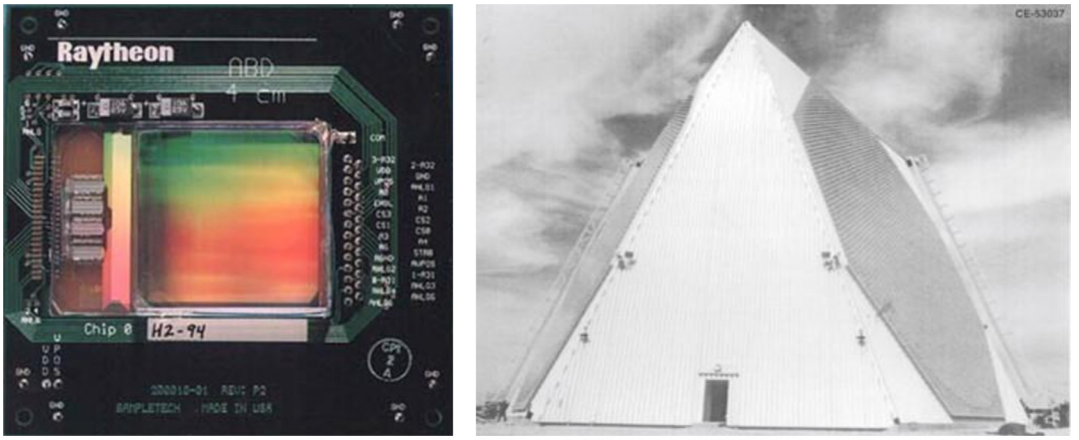

Fig. 6 (a) Early Raytheon OPA with 40,000 phase shifters on 1-μm pitch and (b) Pave Paw Search Radar.

there is less LC material between the electrodes. Polymer network LC-based beam steering can switch 300 faster than standard nematic LC beam steerers.[19,20]

2.1.2 *EO crystal modulo 2π OPAs*

A thin, modulo 2π, beam scanner consists of an optically active layer sandwiched between electrodes. The physics of EO crystal index change will be discussed later when bulk EO crystal-based beam steering is discussed. The optically active area may be either linear, in which case it is called the Pockels[21] effect, or quadratic, in which case it is called the Kerr effect.[22] Voltages are applied to change the refractive index of the active layer, in order to delay the incident light for at least one wavelength. Any types of active materials (a material that has a change in the index of refraction when a voltage is applied), such as LCs, EO crystals, or quantum dot material can be used as the active layer.

Figure 7 shows the performance of a particular potassium tantalate niobate [$KTa_{0.65}Nb_{0.35}O_3$ or KTa1-xNbxO3 (KTN)]-based modulo 2π scanner before and after applying voltages. The devices used in this figure are configured to mitigate fringing field effects and can show an efficiency higher than 90% in steering to 12 and 20 deg. With conventional addressing approaches, not designed to mitigate fringing field effects, such wide steering angles cannot be obtained.[23] In contrast, using fringing field mitigation techniques for a 0.3 birefringence LC, 91% steering efficiency can be achieved only at 3-deg deflection, as shown previously in Fig. 5.

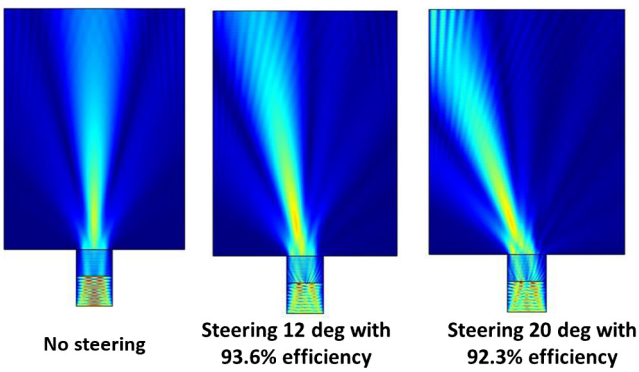

Fig. 7 EO crystal-based beam steering with fringe field mitigation.

One of the advantages of thin EO crystals, or modulo $2\pi n$ LC beam steering devices, over bulk EO crystal beam steerers is that they can support much larger apertures (up to 15-cm in diameter). They will be limited to the size of a wafer until it is possible to stitch larger electronic devices together. The eventual size of these devices is speculative at this time. The above results are simulations not yet from real devices.

2.1.3 *Quantum dot modulo 2π OPAs*

Another active medium that can be considered for modulo 2π beam steering is quantum dots.[24,25] Quantum dots have the advantage that both polarizations can be changed based on applying voltage rather than just one polarization, and they can react fast, similar to EO materials, and much faster than LCs. To date, not much has, however, been published using quantum dots for index change, but recently Portland, Oregon based Inv3ctus, Inc. has been granted a patent on a nonmechanical beam scanning technology employing a quantum dot phased array (QDPA).[26] These devices have the potential to achieve high-refractive index change, therefore, the ability to cause a suitable OPD while using a thin active layer. Most of the work to date has focused on developing the QDPA material to allow the generation of a large OPD with a thin material layer.

The patented design is based upon research that has been conducted in stealth mode, so the only reference for most of the work is the patent. The technology employs specially formulated quantum dots, and some clever architecture wherein the materials can be stimulated to produce a suitable phase delay that may enable beam steering/beam scanning over wide angles with high efficiency, at switching speeds in excess for 30 MHz, using tens of volts, or less, to drive the arrays.

A quantum dot, variable refractive index optical phased array (QDPA) element comprises a structure, which includes quantum dots having discrete energy levels, a dielectric matrix surrounding the quantum dots, and an electron source to inject and discharge electrons into and from the quantum dots through the dielectric matrix to generate and control the

relaxation rate of excitons. The quantum dots are converted into anions by injection of an electron or converted into cations by the discharge of an electron varying the refractive index of the structure. The resulting permittivity and permeability attributes of the quantum dots, as a result of the controlled carrier concentrations, generate a refractive index change without an accompanying absorption increase when the incident photon energy is below the bandgap energy of the quantum dots. Specifically, when an exciton is generated in an isolated quantum dot, an outermost shell orbital (i.e., singly occupied molecular orbital) is newly formed on the outside of the outermost shell orbital [i.e., highest occupied molecular orbital (HOMO)] of the quantum dot. Because the quantum dot is surrounded by a dielectric material, an increase in the refractive index variation is achieved. Inversely, when an exciton relaxes within the quantum dot surrounded by the dielectric, the outermost shell orbital (i.e., HOMO), a similar change in the refractive index is generated.

A typical transmissive QDPA array consists of two glass substrates with thin transparent indium tin oxide layers on opposing surfaces to apply an electric field. The QD-dielectric layer is coated on each plate. As the voltage is varied in a local area of the array, excitons are generated and the relaxation rate controlled resulting in a continuously variable refractive index within each phase shifter. With the proper voltage profile, the wavefront vector can be precisely controlled using modulo $2\pi n$ OPD techniques.

Theory of operation. Light incident on the quantum dot causes the vibration of an electron shell by the electric field. The vibrating electron then re-emits light. The emission process is related to Einstein's B-coefficient, and some duration of time is required from excitation to emission even in a nonresonance region. The light propagates while repeating the excitation and emission. The time required for the excitation and emission determines the phase velocity V_P of light propagation where C is the light velocity in a vacuum, V_P/C is the real part of the complex refractive index that is to be varied in the present invention.

The refractive index is related to the molecular polarizability through the Lorentz–Lorenz equation as given below:

$$\frac{n^2-1}{n^2+2}V_{\text{mol}} = \frac{4\pi}{3}N_A\alpha = R_0, \tag{7}$$

where n denotes a refractive index, N_A denotes Avogadro's number, and α denotes polarizability. Since $\rho = M/V_{\text{mol}}$, where V_{mol} denotes a volume per mole ($N_A = 6.02 \times 10^{23}$), the above equation can be rewritten as

$$\frac{n^2-1}{n^2+2}\frac{M}{\rho} = \frac{4\pi}{3}N_A\alpha, \tag{8}$$

where M is a molar mass (mass per mol) and ρ denotes a density.

When an electron is injected into a quantum dot of nanoscale size, a new orbital is formed, and Coulomb repulsion markedly changes the potentials of HOMO and LUMO, lowest unoccupied molecular orbital, and the HOMO–LUMO gap. It follows that the polarizability is significantly varied by these effects. The injected electron is trapped by the quantum dot by making the LUMO of the dielectric matrix higher than the LUMO of the quantum dot. Where the electron is discharged from a quantum dot, a new orbital is not formed, and the index variation is small compared with the case of the electron injection; albeit still significantly larger than conventional methods.

QDPA technology discussion.

1. The carrier is generated in the quantum dot in the structure.
2. The refractive index variation is maintained as long as the carrier remains in the quantum dot.
3. The QDPA element can generate a large refractive index variation in the transparent region.
4. In the QDPA, the energy levels of the quantum dots are discrete, with the result that the number of electrons that can be present in a single energy level is as small as to be counted. Therefore, when a carrier is newly generated in the quantum dot, it occupies the energy level where an electron has not been present. Also since the energy levels of the quantum dot are discrete, the peak of the absorption spectrum has a small width, which implies that a transparent region is broad.
5. The refractive index of the QDPA is not changed in the dielectric matrix other than the quantum dots, with the result that an average refractive index variation is increased as a whole with an increase in the packing density of the quantum dots.

2.1.4 *Chip scale T/R module based OPAs*

There has been rapid progress in addressing larger and larger arrays of transistors on a chip. For a 2-D array at 1550 nm wavelength, each T/R module has to be 0.75 μm $\times$ 0.75 μm on the surface of the apertures, which is very small. In today's technology, this is impractically small. As a result, the optical community has started developing OPAs that are space-fed and one dimensional at a time rather than working on T/R module-based OPAs. A space-fed array changes the phase of an optical beam passing through it, which results in steering the optical beam. It could be possible, in the relatively near term, to do T/R modules in one direction while using a different nonmechanical approach in the other direction.

Chip-scale OPAs are being pursued.[27] The fundamental physics of OPAs are the same whether one uses a chip to create OPD or uses space-fed birefringent LCs. The chip approach may not, however, have fringing field issues. The approach shown in Ref. 27 creates OPD and uses modulo 2π beam steering. This particular chip is 64×64, with a pitch of 9 μm $\times$ 9 μm, making the array $\sim$576 $\times$ 576 μm. The individual antenna radiators inside a pixel are 3.0-μm in length and 2.8-μm in width. If 3 μm is used as the size of the radiator, and 1.5 μm is the wavelength, steering can be done to about 1/8th radian or about 7 deg. Assuming magnifying this steering to a 10-cm beam, this implies a magnification of about a factor of 174, reducing the 7-deg steering angle to 0.04 deg. Over time the steering arrays will become larger, and the individual steering elements will become smaller. Sun et al.[27] only discussed transmitting, not receiving, which is another required growth area. A second early

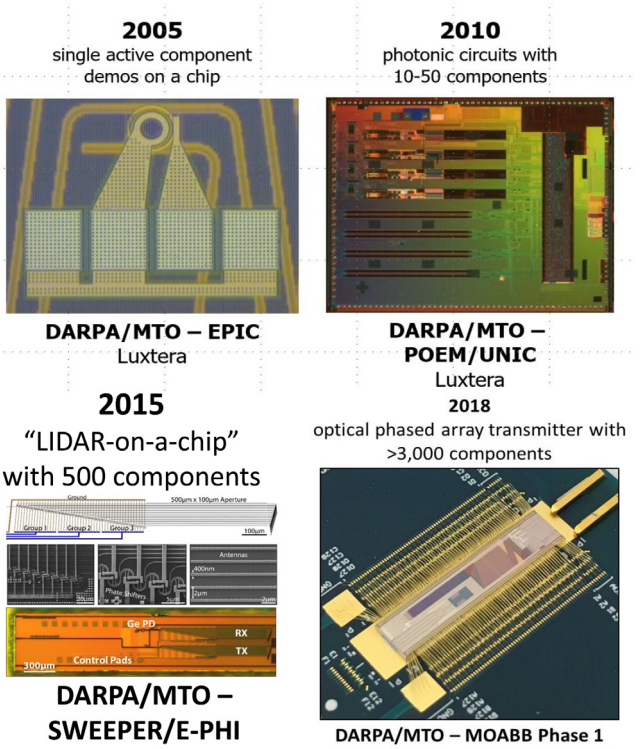

Fig. 8 Progression of DARPA chip scale programs.

chip-scale OPA[28] uses random element pitch to reduce sidelobes but is also a tiny chip, shown in the lower left of Fig. 8. Often when phased array individual elements are larger than a wavelength, the spurious sidelobes can occur. Another way to consider this is that the largest FWHM angle that can be steered to without significant sidelobes is limited by the size of the individual phase shifters. Since steering is only in one direction, and higher efficiency than 50% (half max) is desired, it is necessary to restrict the steering angle to about one-fourth of that value. It is likely that nanofabricated phased arrays will become an interesting option for steering to small angles, using magnification after steering.

More recent progress in chip-scale OPA is discussed in Ref. 29. The planned progression of MOABB is shown in Fig. 9. Lockheed Martin was one of the MOABB contractors, with support from the University of California at Santa Barbara and Davis. They got the spacing down to 1.3 μm, allowing steering up to ± 10 deg. Keeler,[30] the DARPA program manager, showed progress in increasing chip count. Phase II and III of MOABB will progress the chip count higher, as can be seen from Fig. 9. Columbia University and Analog Photonics are two contractors of phase II of the MOABB program.

It can in instructive to compare T/R module-based phased arrays for radar to those of lidar. Traditional radar-based phased arrays have individual phase elements that are at half-wavelength spacing or smaller. Consider an X-band radar at 10 GHz, the wavelength is 3 cm. Wavelength spacing for individual phase shifters with a 3-cm wavelength would mean the pitch between individual phased array elements is no >1.5 cm (half the wavelength spacing). It is possible to build and address individual RF T/R modules that are 1.5 cm $\times$ 1.5 cm on the radiating/receiving surface. To build a square radar aperture that is 75 cm $\times$ 75 cm, it would take a 50×50 array of T/R modules that are 1.5 cm on a side, requiring 2500 individual elements. If this array is round, instead of square, the number of elements would decrease to about 2000 elements.

Consider a similar OPA based on T/R modules. Assume an optical wavelength of 1.5 μm. For half-wavelength pitch, this would require 0.75 μm between elements. Optical apertures usually are not as large as microwave apertures, so one can assume the optical aperture is 30 cm $\times$ 30 cm. To build this, aperture would require 400,000 elements in each direction. This would require a total of 160,000,000,000 (or 1.6×10^{11}) T/R modules for a square aperture, or about 1,250,000,000,000 (1.25×10^{11}) elements for a round aperture. It would be possible to use two crossed one-dimensional arrays. In that case, only 800,000 elements would be needed, which still is a large number. To put these numbers in context, consider that the iPhone 6 in 2015 had 2 billion transistors on a chip, whereas a Pentium 4 in 2001 had 2 million transistors.[31] This is a factor of 1000 increase in 14 years.

Individual T/R module-based phased arrays will come sooner for near range applications, such as an autolidar, which use smaller apertures. Assume a 1-cm diameter aperture. The required number of elements for 2-D addressing with 0.75-μm elements is only 140 million elements are required, which could be reasonable in the relatively near term. If the steering angle is reduced by doubling the spacing between elements then only need one fourth as many are required. This is an area that could be promising over the next decade, especially with the significant money autolidar companies can put into the area.

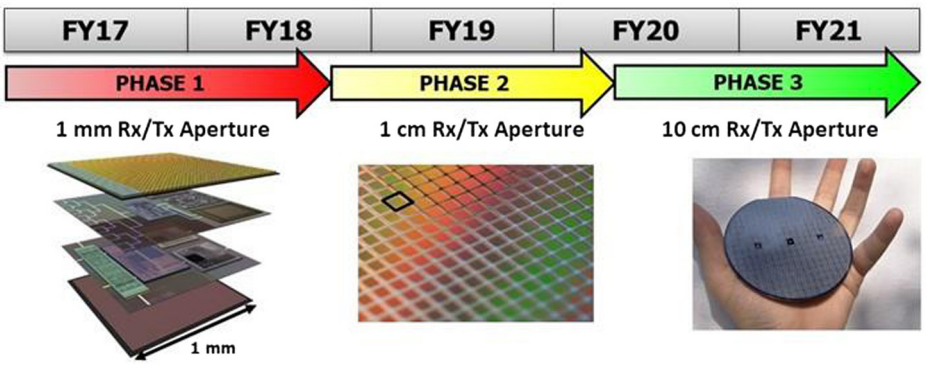

Fig. 9 MOABB phases.

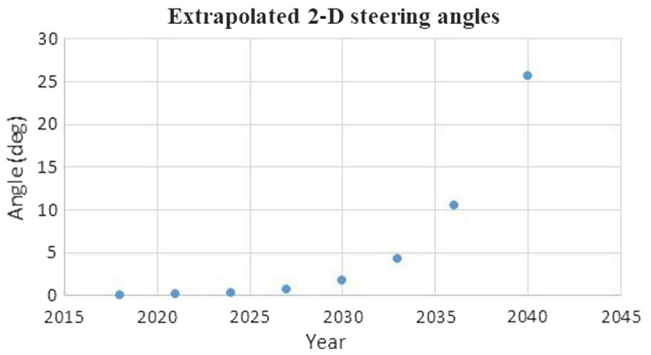

Fig. 10 Extrapolated chip scale steering angles for a 10-cm aperture.

It is interesting to extrapolate from Fig. 8, where it states the Sweeper program had 500 components, and the MOABB phase I program had 3000 components. This comparison is done for a 10-cm diameter aperture. This increase occurred just over 3 years. At the same rate of increase, by 2021 that would have 18,000 elements, which will be enough to do beam steering in a single dimension over ± 15 deg.

The other possibility would be to use these elements in two dimensions but combine chip-scale beam steering with a large-angle, step-stair approach, such as polarization-birefringent gratings, discussed below. This extrapolation is shown in Fig. 10.

2.2 *True Time Delay EO Crystal Steering Approaches*

2.2.1 *Steerable electro evanescent optical refraction*

Davis et al.[32] suggested coupling light into a waveguide whose cladding is LC. The electric field is applied on the cladding to deflect the beam, and finally, the deflected beam is extracted from the waveguide. In this method, deflecting to two dimensions is possible, but the beam should be narrow enough to couple to a guiding mode. This device uses LCs as an active cladding layer in a waveguide architecture, where light is confined to a high-index core, and the evanescent field extends into the variable-index LC cladding. This allows substantial optical-path delays, about 2 mm; so for small apertures, it is a true-time-delay approach, eliminating the need for a modulo $2\pi n$ resets. There is, therefore, no fringing field issue, because there are no resets.

Because the LC layer is thin, these devices can be relatively fast, under 500 μs in response time. In-plane steering is accomplished by changing the voltage on one or more

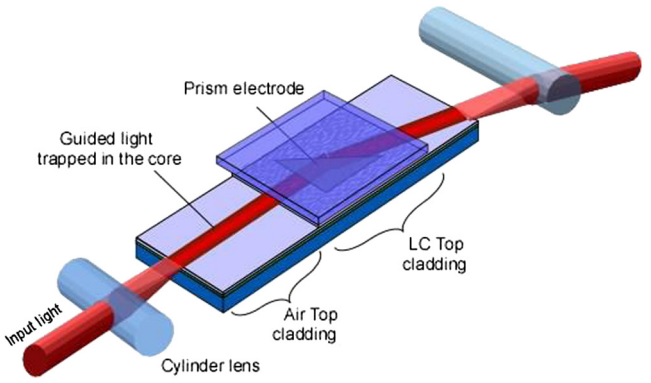

Fig. 11 SEEROR beam steering basic design.

prisms filled with LCs, as shown in Fig. 11.[33,34] Out-of-plane beam steering is based on the waveguide coupler designed by R. Ulrich at Bell Labs in 1971,[35] which is shown in Fig. 12. In any waveguide, if the cladding is too thin light will leak out of the guided mode. In a planar-slab waveguide, Snell's law gives the propagation angle of the escaping light since it is possible to tune the effective index of the waveguide, it is, therefore, possible to tune the angle of the escaping light. This waveguide-based LC beam steering can steer rapidly in one direction over wide angles, such as 40 deg. In the grating-out-coupled-dimension, the deflection angle is more limited, to $\sim$15 deg in either direction. One main limitation of this technique is the size of the apertures, which will be limited to <1 cm on a side, or less. Currently, the loss using this technique is relatively high, on the order of 50%. (The company making these devices has been purchased by analog devices, which has an interest in auto lidar applications. This will likely mean additional money will be invested in the engineering to bring this loss down, and to make these steering devices inexpensive. Making this approach an attractive beam steering technique when small apertures are applicable.)

2.2.2 *Bulk EO crystal beam steering*

Römer and Bechtold[36] investigated the characteristics, properties, speed, accuracy, and the advantages and drawbacks of the EO and acousto-optic laser beam scanners and compared them to mirror-based mechanical deflectors. Since the optical deflectors have high angular-deflection velocities but small deflection angles, compared to mechanical scanners that have low speed but larger deflection angle, Römer and Bechtold suggested arranging an optical deflector and a mechanical scanner in series to take advantage of the benefits of both systems.

Fang et al.[37] and Chiu et al.[38] designed a nonrectangular bulk EO crystal scanner, as per the trajectory of the laser beam inside the crystal. They suggested reducing the width of the beam inlet side of the crystal to increase the EO scanning sensitivity. They examined the performance of their horn-shaped bulk EO crystal scanner—analytically as well as experimentally—and compared it to the rectangular bulk EO crystal scanner.

Scrymgeour et al.[39] have worked on a horn-shaped $LiTaO_3$ wafer. They used EO imaging microscopy to pattern the ferroelectric domains in the shape of a series of prisms whose refractive index is electric field tunable through the EO effect. They reached to 1.80 degrees of deflection per kV, and a maximum deflection of 14.88 deg for a 632.8-nm extraordinary polarized wave and 0.51 degree of deflection per kV and a maximum deflection of 4.2 deg for ordinary polarized light.

Casson et al.[40] demonstrated a beam scanner based on a bulk lithium tantalate crystal to steer a laser beam from the visible to the infrared region, which had a response time on the order of GHz. They reversed the ferroelectric domains in a prism-shaped pattern by applying an electric field of 21 kV/mm at room temperature. They showed that the scanner is capable of steering wavelengths from 400 to 5000 nm, but the steering performance varied from the maximum deflection angle of 13.38 deg at 1558 nm to 16.18 deg at 632.8 nm. They finally calculated the EO coefficients ($r31$ and $r33$) of lithium tantalate from the deflection angle for each

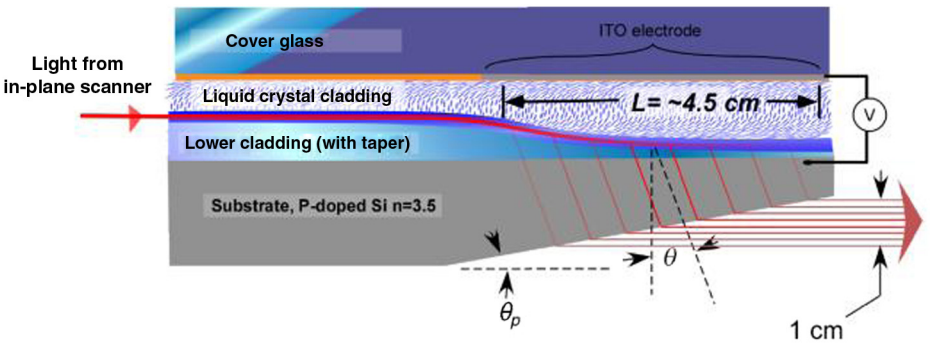

Fig. 12 Out coupling approach for the second dimension using steerable electro evanescent optical refraction beam steering.

Fig. 13 EO crystal beam steering in both dimensions.

wavelength and showed those parameters decrease for longer wavelengths.

A key constraint on bulk EO crystals is crystal thickness, which is proportional to the required voltage, for the linear EO effect. Kilovolts will be required for bulk EO crystal-based steering. Lithium niobate has been used a long time for steering beams, but it has a low EO coefficient, so it requires a higher voltage than some newer EO crystal materials. More recently, high-EO coefficient materials, such as KTN, $BaTiO_2$, Pb(Zn1/3Nb2/3)O3, strontium-barium niobate (SBN), and Pb (Mg1/3Nb2/3) O3-PbTiO3 (PMN-PT) have been investigated because of higher EO coefficients and the potential for lower required voltage.[41–45]

A critical issue for bulk-beam steering is the required voltage. There is a trade-off as the steered beam gets larger, so does the voltage, but small beams require magnification, which reduces steering angle. Also beam walk-off results from deflecting the beam inside the crystal, so for larger angles a portion of the beam might hit the side of the crystal. This requires a larger crystal, increasing the required voltage, to obtain a certain electric field. Beam walk-off is more of an issue for the first dimension steered when steering both dimensions, because the first dimension steered will have a long path in the second crystal, after being steered in the first crystal. For a 20-mm-long crystal to steer each dimension then by the end of the second crystal, there should be an effective 30-mm walk-off length. In the first 20-mm-long crystal, there will be an effective 10-mm walk-off length because the steering occurs gradually over the length of the crystal. The angle obtained in the first crystal continues into the second crystal, as shown in Fig. 13.

Figure 14 shows the beam bending in the first crystal and then going straight in the second crystal, as would happen to the beam steered in the first crystal. Therefore, the beam in the second crystal can hit the sidewall, especially if the beam width is an appreciable percentage of the crystal thickness. The steering in the first dimension has already occurred when light hits the crystal that steers the second direction. In the dimension steered by the first crystal, the second crystal will have to be wider to avoid the beam hitting the sidewall due to the beam walk-off. The OPD required to steer to a particular angle/aperture product remains the same for a given crystal, regardless of the width of the crystal used.

It is possible to think of an EO crystal as a capacitor. The capacitance of an EO crystal with the length of L, the width of w, and height of d is given by

$$C = \frac{\varepsilon_{r_{ij}} \varepsilon_0 L w}{d}, \tag{9}$$

where ε_0 is the permittivity of free space. The dielectric constant ($\varepsilon_{r_{ij}}$) in Eq. (9) can be different for different crystal orientations and for different crystals. To keep the capacitance low, a low-dielectric constant would be desirable, but a high-dielectric constant can allow a larger steering angle per applied voltage, which may be desirable.

One way to steer to a certain angle, using a prism-type OPD profile, will be to create an OPD on one side of the crystal, preferably with a linear prism profile in OPD across the crystal. One side of the crystal will have a maximum OPD, and the other side will have zero OPD. This change in OPD across a crystal creates a tilt to the outgoing wavefront. The change in OPD is given by

$$\text{OPD} = \Delta n L, \tag{10}$$

where L is the length of the crystal, or the area of the crystal with a changed index of refraction, and Δn is the change in the index of refraction. Although it is possible to develop a larger OPD using a longer interaction length, up to the size of the largest available crystal, it is desirable to create a larger Δn instead of a larger interaction length as the method of developing a given OPD. A larger interaction length not only makes the beam steerer larger but also creates more of a walk-off issue, where a portion of the beam could hit the sidewall of the crystal unless the beam is kept very small compared to the crystal size.

The amount of OPD generated determines the angle/aperture product for beam steering. A wider aperture means steering to a smaller angle but does not change the angle/aperture product.

Because of the higher index of refraction, it will not be necessary to steer to as large an angle inside the crystal to generate this angle upon leaving the crystal. Snell's law can be used to determine what steering angle inside the crystal is required. For small angles, Snell's law can be written as

$$\frac{\theta_d}{\theta_i} \approx \frac{n}{n_0}, \tag{11}$$

where θ_d is the desired deflection angle in the air, θ_i is the deflection angle inside the crystal, n_0 is the refractive index of air, which is considered as 1, and n is the refractive index of the EO crystal. Solving for θ_i:

$$\theta_i \approx \frac{\theta_d}{n}. \tag{12}$$

The approximate index of refraction (n) for KTN crystal is 2.29, for PMN-PT crystal is 2.47, and for SBN is 2.35. As seen, using these values reduces the required internal steering angle (θ_i) for prism-type steering.

It is possible to generate a refractive index change (Δn) either by linear or quadratic EO effect. Some EO crystals exhibit a quadratic EO effect (or Kerr effect) below and above the Curie temperature. The EO crystals can also exhibit a linear EO effect (or Pockels effect) below the Curie temperature if they do not have a centrosymmetry in their crystalline structure.[46] Since the possible lack of centrosymmetry in the crystalline structure will disappear above the Curie temperature, the Pockels effect does not exist above the Curie temperature.[47]

Generally, if a crystal exhibits both Kerr effect and Pockels effect below the Curie temperature, the Pockels effect will be about ten times stronger than Kerr effect. The Pockels effect crystals need to be poled, but Kerr effect crystals do not need to be poled. The linear EO effect creates a Δn as

$$\Delta n = -\frac{1}{2} n^3 r_{ij} E_j, \tag{13}$$

where r_{ij} is the linear EO effect coefficient in an appropriate direction, E_j is just voltage divided by crystal thickness in an appropriate direction, and n is the refractive index of the crystal.

The change in the refractive index by Kerr effect[48] is as follows:

$$\Delta n = -\frac{1}{2} n^3 S_{ij} E_j^2, \tag{14}$$

where s_{ij} is the quadratic EO (Kerr) effect coefficient in an appropriate direction, E_j is the applied electric field in an appropriate direction. As seen, Eq. (14) is similar to Eq. (13), except for the nonlinear EO effect coefficient (S_{ij}) and the square electric field (E_j^2) term.

2.3 *Steering Using Traditional Gratings*

The grating equation for normal incidence is given as

$$\sin\theta = \frac{m\lambda}{d}, \tag{15}$$

where m is the diffraction order and d is the pitch of the grating. For small angles, the steering angle is proportional to wavelength. It is possible to change the steering angle by changing wavelength. Therefore, for an EO system capable of changing wavelength, nonmechanical beam steering can be done using the dispersion of a grating or other dispersive elements. The MOABB program, developing chip scale OPA devices, cannot at this time have enough addressing elements to steer both dimensions based on chip scale OPAs, so it relies on wavelength dispersion and wavelength change to steer the second wavelength, as discussed early when chip scale OPAs are summarized.

2.3.1 *Volume holographic gratings*

Volume (thick) holograms offer the potential to implement large-angle steering with high efficiency.[49] Once the hologram is developed, it will diffract an incident signal beam in the direction of the reference beam, thereby steering the signal beam while being almost transparent to beams coming into the volume hologram layer at different angles. The method of steering is to change the input angle slightly, resulting in a significant change in the output angle.

Through the use of multiple holograms, multiple discrete steering angles can be addressed. The number of steered angles increases linearly with the number of holographic gratings. This is the reason that holographic-beam steering has lost its popularity compared to polarization birefringent gratings (PBGs). In the 1990s, the main wide-angle-beam steering approach was holographic gratings, which were made by Leon Glebov at the College of Optics and Photonics, and the company he started called Optigrate. Holographic gratings use high-fidelity, rugged, photothermal glass[50] for writing holograms. Each glass holographic grating can have more than 99% efficiency.[51] When two holograms are written in a single piece of glass, the efficiency can still be higher than 98%.[52]

Many layers of holographic glass can be placed back-to-back with relatively low losses. For example, eight holograms in each direction, azimuth, and elevation could be used. If each hologram steers to an angle separated by 5 deg from the adjacent angle, then there is an entire field of regard of 40 deg, broken up into eight zones of 5 deg each. The incoming light is only diffracted by the holographic grating that has light input at the proper angle and wavelength. There is no additional diffractive loss using more gratings. However, using a larger number of volume holograms introduces reflection, scattering, and absorption losses. In addition, the thickness of the grating stack increases, and there will be a limitation on how thick a piece of glass can be used to contain gratings. Each grating is set to receive light from a small angle, and to steer it to a specific larger angle, dividing the steering into zones. Steering inside of each zone is referred to as filling each zone. This requires the use of a second beam steerer in each dimension after

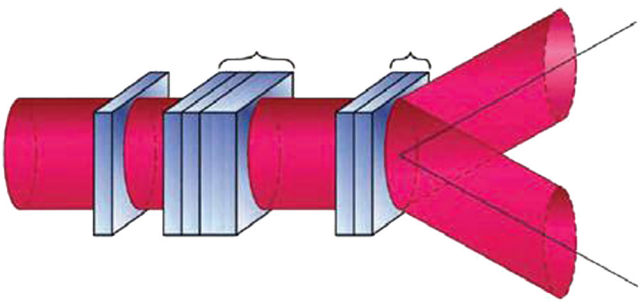

Fig. 14 Wide angle beam steering using holographic glass.

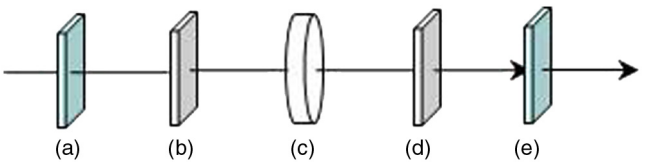

Fig. 15 A basic setup of QHQ stack: (a), (e) polarizer; (b), (d) quarter-wave plate; and (c) half-wave plate.

the stack of volume holograms. This wide-angle steering approach, therefore, requires two moderate-angle continuous beam-steering devices, one before (for zone selection) and one after (for zone fill) the stack of volume holograms. This steering approach has demonstrated continuous beam steering over a field of regard >45 deg.[12,53]

This architecture is shown in Fig. 15. It would be possible to use this technique to steer both polarizations of light, but as it was implemented, it would mean doubling the number of beam steering elements. The small-angle LC beam-steering elements used to address the volume holograms were polarization dependent. Thus for an 80-deg field of regard and 5 deg per step, there would need to be 16 gratings in each dimension. Even at 0.5% loss per grating that would mean a 16% loss when both dimensions are included. Using this method, it is critical to reduce losses per stage to a minimum if large-angle deflection is desired at high efficiency. A single piece of the grating is 1- to 2-mm thick. This can cause limited walk-off issues in a large stack, due to 2- to 4-cm thickness for 20 gratings. Walk-off means the beam can move off the active area of the substrate or can hit the sidewall because it is essentially steered inside of a tunnel.

Using volume holograms in conjunction with small angle continuous steering approaches allowed steering continuous and efficient steering over a 45-deg cone. (This demonstration was conducted as part of the DARPA steered angle beams program, technically monitored by Dr. McManamon. The data from this demonstration may not have been published in an achival journal), but it was abandoned once polarization-birefringent gratings became available.

2.3.2 *Acousto-optical beam steering*

Acousto-optical beam deflection devices are an example of using writable gratings to deflect light. A sound wave can create a Bragg grating in a material, and that grating can deflect light. A different Bragg grating can be written in the time it takes a sound wave to travel from one side of a crystal to the other side so that steering time will depend on the size of the crystal, and the speed of sound in that material. By changing the frequency of the acousto-optical wave, the grating period can be changed. The tilt angle will be given by

$$\theta \approx \frac{\lambda}{\Lambda}, \tag{16}$$

where Λ is the period of the acoustic wave and λ is the optical wavelength.[54,55] Steering efficiency decreases quadratically with increasing wavelength, so a stronger acoustic beam is required to deflect longer wavelengths. This can result in high power being required for the beam deflector.

3 Phased-Based Nonmechanical Beam Steering (Based on the Seminal Paper of Pancharatnam)

Nonmechanical beam-steering approaches discussed until now rely on creating OPD. There is an alternate approach that directly creates a phase delay. Figure 15 shows the optical model of the quarter-wave plate, half-wave plate, quarter-wave plate (QHQ) device first described in the paper by Pancharatnam. A light beam passes through a polarizer, a quarter-wave plate ($\lambda/4$ plate), a half-wave plate ($\lambda/2$ plate), another quarter-wave plate, and another polarizer. The director profile of LC polarization gratings: (a) top-view, and side-view in the zero (b) high and (c) voltage cases, as shown in Fig. 16. Linear polarized incident light becomes circular polarized after the first $\lambda/4$ plate, which can be defined as the electric field of E_{in} according to Jones calculus notation:

$$E_{\text{in}} = \begin{pmatrix} E_{x\text{in}} \\ E_{y\text{in}} \end{pmatrix} = \begin{pmatrix} E_{x\text{in}} \\ iE_{x\text{in}} \end{pmatrix}. \tag{17}$$

For convenience, it is assumed to be a right-hand circular polarized light. $E_{x\text{in}}$ and $E_{y\text{in}}$ are vector components of the electric field along the x axis and y axis, respectively. The transmitted light E_{out} is defined as a linear mapping of the incident light E_{in} by a Jones matrix:

$$E_{\text{out}} = \begin{pmatrix} \cos\beta & -\sin\beta \\ \sin\beta & \cos\beta \end{pmatrix} \begin{pmatrix} 1 & 0 \\ 0 & e^{i\varphi} \end{pmatrix} \begin{pmatrix} \cos\beta & \sin\beta \\ -\sin\beta & \cos\beta \end{pmatrix} \begin{pmatrix} Ex_{\text{in}} \\ iEx_{\text{in}} \end{pmatrix}, \tag{18}$$

where β represents the angle between the slow axis of the half-wave plate and the x axis, and φ is denoted as the phase retardation of the half-wave plate, which is equal to π. The final relationship can be simplified as

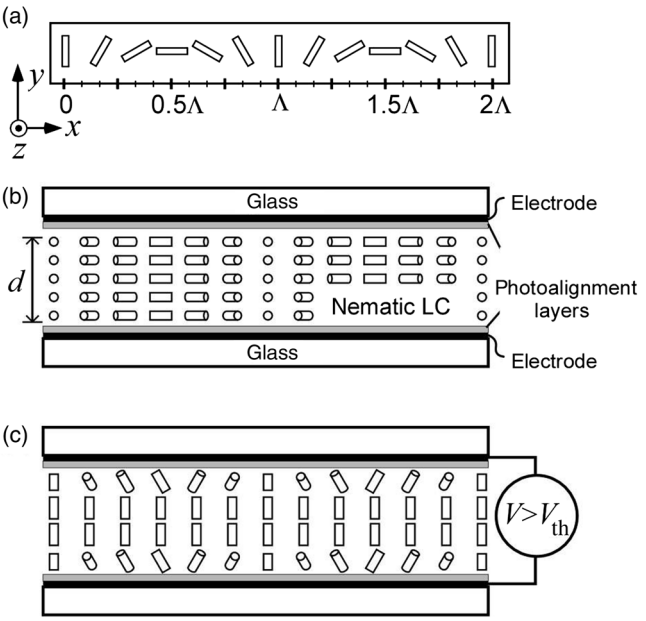

Fig. 16 The director profile of LC polarization gratings: (a) top-view, and side-view in the zero (b) high and (c) voltage cases.

$$E_{\text{in}} = \begin{pmatrix} E_{x\text{in}} e^{2i\beta} \\ iE_{x\text{in}} e^{2i\beta} \end{pmatrix}. \tag{19}$$

In the last expression, the transmitted light is a left-hand circular polarized light with a common phase factor $e^{2i\beta}$. The phase of the transmitted circular light can be accurately controlled by the azimuth angle β. If β varies laterally from 0 to π the spatial phase profile of transmitted light will vary horizontally from 0 to 2π. For an LC cell with an in-plane director, the azimuth angle linearly rotating from 0 to π and the total OPD across the cell agreeing with the half-wave retardation for the design wavelength, then the final spatial phase profile of transmitted light will linearly change from 0 to 2π. By duplicating this spatial director configuration repeatedly, an LC grating without any flyback or reset can be created.

It should be noted that the cell is only one half-wave OPD thick and importantly, the flyback, or reset, is eliminated in this device. The thin cell gap reduces light scatting and adsorption of the LC cell. With this type of device, even though the optical thickness is only half of the wave, it is possible to create a constant, large phase gradient over an aperture size only limited by manufacturing constraints.

3.1 *Polarization Birefringent Gratings*

LC polarization gratings (LCPGs) with near ideal diffraction efficiencies (>99.5%) have been experimentally demonstrated, over a wide range of grating periods, wavelengths (visible to near-IR), and areas.[56,57] Each polarization grating (PG) stage can double the maximum steered angle in one dimension, without major efficiency reductions, so very large steered angles are possible (at least to ±40- deg field of regard). Currently, devices larger than 15-cm in diameter have been fabricated. (These consclusions were based on manufacturing experience by BNS.)[58] A LCPG defects light in one direction when the light is circular polarized one direction, and in the opposite direction when the circular polarization is reversed. Active LCPGs can also be turned on and off. Between each LCPG layer, we place a variable waveplate that changes the handedness of the polarization.

Similar to the birefringent prisms, only a single-stage fine angle steerer is required before the LCPG to achieve continuous wide-angle steering. This is in contrast to volume holographic where wide-angle steering requires two fine-angle steerers, one before and one after the holographic stack of glass. The structure at the heart of these devices is a PG, implemented using nematic LCs (optionally switchable, or polymerizable). The nematic director is a continuous, in-plane, bend-splay pattern established using a UV polarization hologram exposing photoalignment materials. When voltage is applied, the director orients out of the plane, effectively erasing the grating. Diffraction occurs according to the following equations:

$$\eta_{m=0} = \cos^2\left(\frac{\pi \Delta n d}{\lambda}\right), \tag{20}$$

$$\eta_{m=\pm 1} = \left(\frac{1 \mp S_3'}{2}\right) \sin^2\left(\frac{\pi \Delta n d}{\lambda}\right), \tag{21}$$

where η_m is the diffraction efficiency of the m'th order, λ is the wavelength of the incident light, and $S_3' = S_3/S_0$ is the normalized Stokes parameter corresponding to the ellipticity of incident light. The grating equation applies. Note that only these three orders are possible and that when the retardation of the LC layer is half wave ($\Delta n d = \lambda/2$), then 100% of the incident light can be directed out of the zeroth order. Note further that when the input polarization is circular, then all light can be directed into a single first order, with the handedness ($S_3' = \pm 1$) selecting the diffraction order (see Fig. 19). When Fig. 19 refers to high voltage, it only means tens of volts. A single LCPG can be considered the key component within a digital beam steerer with three possible directions ($\pm\theta$ and 0). For the nondiffracting case, an applied voltage reduces the effective birefringence toward zero ($\Delta n \to 0$).

LCPGs may also be fabricated with polymerizable LCs, also known as reactive mesogens, and would, therefore, be fixed indefinitely. The practical advantages of these passive PGs (over the switchable or active PGs) are that they tend to manifest less scattering losses and allow for smaller grating periods.[59]

The real-world realization of near 100% efficiency circular LCPGs took substantial time and effort. The feasibility of 100% diffraction efficiency in thin gratings recorded by two circularly polarized coherent waves was suggested in 1983.[60,61] The concept of using photoaligned, bulk nematic LCs for LCPGs was identified by Zeldovich and Tabiryan[62] in invention disclosure and conference appearance,[63] as well as by Crawford et al.[64] in a patent application. The Crawford team's subsequent journal publications[65,66] only offered a first-order efficiency of <10%. Escuti et al.[67] were the first to disclose the methods needed to fabricate an LCPG with an efficiency higher than 99% in a patent application filed in 2005, for both switchable and polymer LCPGs.

Sarkissian et al. reported 12.7% to 18.7% steering efficiency.[68] Escuti and Jones[56,57] and Provenzano et al.[69] published near 100% efficiency in the broader literature. A detailed historical analysis of some of these critical contributions (and many more) may be found in multiple Refs. 70–72.

Kim et al.[73] published an article using LCPGs in nonmechanical beam steering, while working under Dr. Mike Escuti. They introduced high-efficiency coarse beam steering modules using both active and passive PG architectures. Various designs and improvements have been studied subsequently by this team,[74–76] by Tabiryan et al.,[71,72] and by Wu et al.[77,78] A patent application[79] filed in 2009 was issued to NCSU and BNS, for this family of beam steering with LCPGs.

3.2 *Vertical-Continuous, Optical-Phased Arrays*

LC OPAs usually follow the idea of generating a linear change of OPD across the aperture while using resets to keep the required OPD small. Resets then impose a flyback region, reducing efficiency. As an alternative, the vertical-continuous, optical-phased array (VCOPA) devices discussed here use the same basic physics as the QHQ device of Pancharatnam, discussed earlier. It is a phase-based device rather than an OPD-based device. The difference is the steering angle of a single VCOPA device is variable instead of fixed, like the previously discussed circular birefringent gratings. VCOPA devices also have ~99.5% diffractive steering efficiency, similar to birefringent prisms.

The LCPGs discussed earlier achieve their spiral structure through the use of an alignment layer that has the desired spiral structure. This method obviously does not yield a

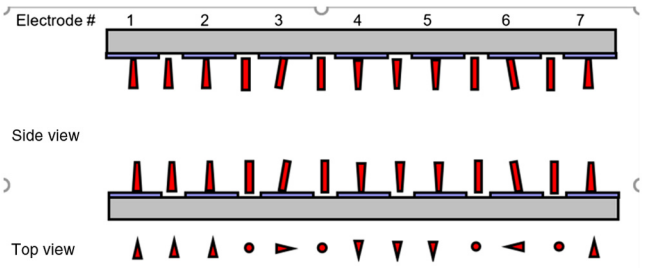

Fig. 17 VCOPA alignment.

tunable device. Kent State has demonstrated a variable device called VCOPA. The basic structure of the device is shown in Fig. 17, by Lei Shi of Kent State.[80] The alignment is approximately vertical at the top and bottom substrates. The alignment is quasivertical alignment because in some domains the alignment is not exactly vertical, but slightly tilts to the left, right, or in and out of the plane of the paper.

For example, the alignment over electrodes #1 and #2, and over the gap between them, is slightly pointed into the plane of the paper. Similarly, the alignment over electrode #3 is slightly pointed to the right, whereas the alignment over electrode #6 is pointed to left, etc. All the other regions' alignment keeps the initial vertical direction. The cell is filled with $-\Delta\varepsilon$ LC materials, so when a voltage is applied to cause an electric field that is vertical in this figure, the LC directors will distribute in the x–y plane. The helical sense adopted is controlled by the slight tilting of the director alignment layer. The tipping of the director to the left and right in Fig. 20 can be controlled by fringing fields resulting from the voltage pattern applied to the in-plane cell electrodes. In this way, the regions tilting to the left or right can be controlled, and the sense of the helix can be electrically controlled. By controlling the voltages applied to the electrodes, the period of the helix can be changed, and a tunable steering angle can be achieved. The main focus of current work on VCOPA is switching speed. The original work had switching speeds on the order of seconds, and it would be desirable to reduce those speeds to the order of milliseconds or less. If speed is sufficient, then this will become a very attractive steering approach. It has high diffractive efficiency, like the birefringent prisms, but will require fewer layers. It is not clear that tunable devices will be manufacturable to steer to as large an angle as the fixed devices, so a future combination of VCOPA with a large-angle step-steering approach similar to birefringent prisms is likely.

4 Nonmechanical Steering of Broadband EO Beams

Trying to steer broadband sensors was first pursued in the late 1980s to early 1990s, not long after starting the efforts to steer narrowband light nonmechanically.[6,81–84] One of the early useful insights was that larger resets are somewhat more broadband, even though it was not proven in a paper until 2005. Reference [7] shows in theory and experiment the effect of larger resets on the broadband nature of the beam steerer.[7] When many avenues were pursued, the best approach for broadband beam steering was, and is, achromatic Fourier transforms (AFT).[85] The full-width half-max diffraction limit of the aperture is

$$\Delta\theta \approx \frac{\lambda}{D}. \tag{22}$$

Gratings steer to an angle proportional to wavelength for small-angle steering as follows:

$$\theta = \theta_0 \frac{\lambda}{\lambda_0}. \tag{23}$$

As seen, a longer wavelength steers to a larger angle, but the goal is to have all the light leaving one aperture hit a specific other aperture. Therefore, it is necessary to eliminate dispersion. A steering angle is reduced by magnification as follows:

$$\theta_M = \frac{\theta}{M}, \tag{24}$$

where M is the magnification. For a magnification by a factor of ten, the steering angle is reduced by a factor of ten. Consider a telescope with magnification that is dispersive as follows:

$$M = M_0 \frac{\lambda}{\lambda_0}. \tag{25}$$

It has a basic magnification but is dispersive, changing the steering angle. Equation (26) shows the elimination of dispersion:

$$\theta_M = \frac{\theta_0 \lambda \lambda_0}{M_0 \lambda_0 \lambda} = \frac{\theta_0}{M_0}. \tag{26}$$

Note that the wavelength dependence has disappeared. To eliminate dispersion in this way, it is necessary to develop a telescope with magnification given by

$$M = \frac{f_1}{f_2}, \tag{27}$$

where f_1 and f_2 are the focal lengths of the two lenses in a simple telescope. One of the focal lengths must depend on wavelength, for example:

$$f_1 = f_0 \frac{\lambda}{\lambda_0}. \tag{28}$$

If f_1 changes, then under normal circumstances, lens #1 no longer focuses at the same spot. This means that the two lenses do not focus on the same spot, so the telescope becomes blurry and is no longer a useful telescope. It is

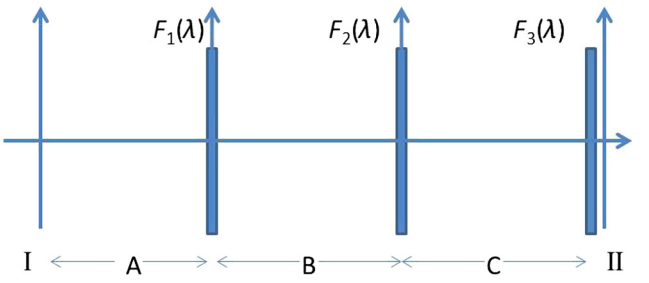

Fig. 18 Lens positions for an AFT.

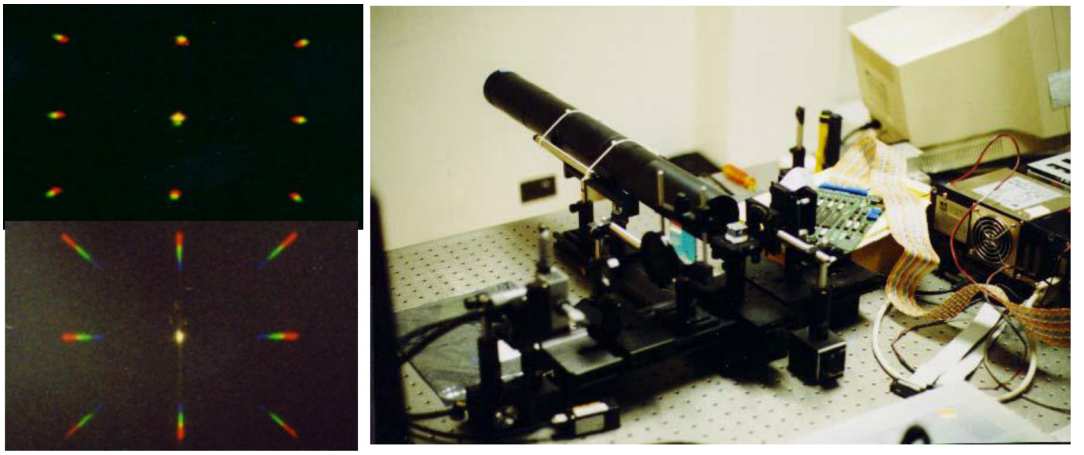

Fig. 19 A broadband beam steering device.

necessary to have a "lens" with variable focal length but a constant back focal distance. The "lens" always focuses on the same spot, even though its focal length changes. An AFT lens can have this property. The magnification amount could be just 1-to-1 as the basic magnification, with dispersion on top of that basic magnification. It could also be a different value if that would be useful in the design.

Figure 18 shows a diagram of the internal make up of an AFT "lens."[85] Only the first two lenses are required, except for image size. One of these lenses is diffractive. It has normal diffractive dispersion. The second lens has dispersion that is the opposite of lens 1 in the AFT, so the opposite of diffractive dispersion. The main challenge in designing the AFT is wavelength operation over a wide bandwidth.

In the 1990s, BNS built a demo device for broadband visible beam steering for the Air Force. It is shown in Fig. 19. The lens was longer than the author wanted but did work over a limited band in the visible light region.

The U.S. Air Force has an interest in compact systems, so making this "lens" longer than 1 foot would limit its usefulness. In Fig. 19, the actual device is shown on the right, and on the left is the uncompensated steering of a point of broadband light on the bottom, and the compensated steering on the top. The compensation was not perfect, but the colors were mostly brought back together.

5 Conclusion

Nonmechanical beam steering has come a long way since the mid-1980s. Initial work was mostly in LCs. There was some acousto-optical work as well. Fringing fields limited the steering angle for LC OPAs. As a result, larger-angle step stare approaches were pursued. The first of those was volume holographic gratings (VHGs). Although VHGs were successful, the number of steering angles was linearly proportional to the number of volume holograms, and continuous small angle steering occurred both before and after the VHGs. More recently, large-angle step steering has been carried out using PBGs. VCOPA uses the same physics as PBGs but can be steering to variable angles. VCOPA has been a very interesting method of steering, but with a slow steering rate (on the order of a second), over angles up to about 5 deg. Work is occurring to speed up the steering time for VCOPA. EO crystals are becoming more promising, using higher-EO coefficient crystals, and novel addressing structures. High efficiency, >90% out to 20 deg, is possible and should be feasible for cm to tens of cm diameter apertures. Chip-scale OPAs are under development but are still at an early stage. At this time, they will be restricted to either one-dimensional steering or small-angle steering, for moderate size aperture. Chip scale OPA progress may be made for small apertures of 1-cm in diameter. Broadband nonmechanical beam steering is far behind narrow-band, nonmechanical beam steering but is beginning to make progress using AFT-based variable telescopes to compensate for dispersion.

References

1. P. F. McManamon and A. Ateai, "Progress and opportunities in optical beam steering," *Proc. SPIE* **10926**, 1092610 (2019).
2. S. Pancharatnam, "Achromatic combinations of birefringent plates," *Proc. Indian Acad. Sci., Sect. A* **41**(4), 137–144 (1955).
3. P. F. McManamon et al., "Nonmechanical steering of the field of view of broad spectral band optical systems," *Proc. SPIE* **5873**, 26–37 (2005).
4. B. Hatcher, "Granularity of beam positions in phased arrays," *Proc. IEEE* **56**(11), 1795–1800 (1968).
5. G. Thalhammer et al., "Speeding up liquid crystal SLMs using overdrive with phase change reduction," *Opt. Express* **21**(2), 1779–1797 (2013).
6. P. F. McManamon et al., "Nonmechanical beam steering for active and passive sensors," *Proc. SPIE* **1969**, 2–10 (1991).
7. P. F. McManamon, J. Shi, and P. Bos, "Broadband optical phased-array beam steering," *Opt. Eng.* **44**, 128004 (2005).
8. J. Goodman, *Introduction to Fourier Optics*, p. 65, McGraw Hill, San Franciso (1968).
9. E. W. Weisstein, "Full width at half maximum," From mathworld—a wolfram web resource, http://mathworld.wolfram.com/FullWidthatHalfMaximum.html (2019).
10. M. I. Skolnik, *Introduction to Radar Systems*, International Student Edition, p. 267, McGraw Hill, New York (1962).
11. J. Frank and J. D. Richards, "Phased array radar antennas," Chapter 13 in *Radar Handbook*, M. Skolnik, Ed., 3rd ed., pp. 13.2–13.3, McGraw Hill, New York (1990).
12. P. F. McManamon, "Agile nonmechanical beam steering," *Opt. Photonics News* **17**(3), 24–25 (2006).
13. P. F. McManamon et al., "Optical phased array technology," *Proc. IEEE* **84**(2), 268–298 (1996).
14. X. Wang et al., "Spatial resolution limitation of liquid crystal spatial light modulator," in *Liquid Crystal Conf., Great Lakes Photonics Symp.*, Cleveland, Ohio (2004).
15. R. M. Matic, "Blazed phased liquid crystal beam steering," *Proc. SPIE* **2120**, 194–205 (1994),
16. P. F. McManamon and A. Ataei, "System, method, and apparatus for electro-optical non-mechanical beam steering," Publication # US2019/0129275 (2017).
17. https://en.wikipedia.org/wiki/PAVE_PAWS (accessed 3 January 2019).
18. https://en.wikipedia.org/wiki/Liquid_crystal_on_silicon (accessed 27 May 2019).
19. R. L. Sutherland, V. P. Tondiglia, and L. V. Natarajan, "Electrically switchable volume gratings in polymer-dispersed liquid crystals," *Appl. Phys. Lett.* **64**, 1074–1076 (1994).
20. L. H. Domash et al., "Switchable-focus lenses in holographic polymer-dispersed liquid crystal," *Proc. SPIE* **2689**, 188–194 (1996).
21. https://en.wikipedia.org/wiki/Pockels_effect (accessed 29 May 2019).
22. https://en.wikipedia.org/wiki/Kerr_effect (accessed 29 May 2019).

23. P. McManamon and A. Ataei, "System, method and apparatus for non-mechanical optical and photonic beam steering," application # PCT/US19/23915, PCT filed (2019).
24. T. Piwonski et al., "Refractive index dynamics of quantum dot based waveguide electroabsorbers," *Appl. Phys. Lett.* **97**, 051107 (2010).
25. B. Çakır, Y. Yakar, and A. Özmena, "Refractive index changes and absorption coefficients in a spherical quantum dot with parabolic potential," *J. Lumin.* **132**, 2659–2664 (2012).
26. J. Albelo and J. LaChapelle, "Beam scanner for autonomous vehicles," 2017, http://patft.uspto.gov/netacgi/nphParser?Sect1=PTO2&Sect2=HITOFF&p=1&u=%2Fnetahtml%2FPTO%2Fsearch-bool.html&r=2&f=G&l=50&co1=AND&d=PTXT&s1=Albelo&OS=Albelo&RS=Albelo (2018).
27. J. Sun et al., "Large-scale nanophotonic phased array," *Nature* **493**, 195–199 (2013).
28. D. Kwong et al., "1 × 12 unequally spaced waveguide array for actively tuned optical phased array on a silicon nanomembrane," *Appl. Phys. Lett.* **99**, 051104 (2011)
29. P. J. M. Suni et al., "Photonic integrated circuit FMCW lidar on a chip," in *19th Coherent Laser Radar Conf.*, Japan (2018).
30. G. Keeler, *Laser Sens. and Commun. Conf.*, OSA Imaging and Applied Optics Congress, Modular Optical Aperture Building Blocks (MOABB), Orlando, Florida (2018).
31. P. J. M. Suni et al., "Coherent lidar-on-a-chip," in *IEEE NAECON Conf.* (2017).
32. S. R. Davis et al., "New wide angle electro-optic laser scanners enable optical sensors on previously inaccessible platforms," in *Imaging and Applied Opt., OSA Technical Digest (CD)*, Optical Society of America, paper AIWB3 (2011).
33. S. R. Davis et al., "Liquid crystal waveguides: new devices enabled by >1000 waves of optical phase control," *Proc. SPIE* **7618**, 76180E (2010).
34. S. R. Davis et al., "New electro-optic laser scanners for small-sat to ground laser communication links," *Proc. SPIE* **8739**, 87390H (2013).
35. R. Ulrich, "Optimum excitation of optical surface waves," *J. Opt. Soc. Am.* **61**, 1467–1477 (1971).
36. G. R. B. E. Römer and P. Bechtold, "Electro-optic and acousto-optic laser beam scanners," *Phys. Procedia* **56**, 29–39 (2014).
37. J. C. Fang et al., "Shape-optimized electrooptic beam scanners: experiment," *IEEE Photonics Technol. Lett.* **11**(1), 66–68 (1999).
38. Y. Chiu et al., "Shaped-optimized electrooptic beam scanners: analysis, design and simulation," *J. Lightwave Technol.* **17**(1), 108–114 (1999).
39. D. A. Scrymgeour et al., "Large-angle electro-optic laser scanner on $LiTaO_3$ fabricated by in situ monitoring of ferroelectric-domain micropatterning," *Appl. Opt.* **40**(34), 6236–6241 (2001).
40. J. L. Casson et al., "Determining electro-optic coefficients for lithium tantalate using an electro-optic scanning device," article, 2001, https://digital.library.unt.edu/ark:/67531/metadc931666/ (accessed 4 June 2019), University of North Texas Libraries, Digital Library, https://digital.library.unt.edu, crediting UNT Libraries Government Documents Department.
41. P. Kumar et al., "Dielectric, piezoelectric and pyroelectric properties of PMN-PT (67:32) system," *Ceramics Int.* **30**, 575–579 (2004).
42. H. Jiang et al., "Transparent electro-optical ceramics and devices," *Proc. SPIE* **5644**, 380–394 (2004).
43. T. Liu et al., "Crystallization kinetics and temperature dependence of energy storage properties of niobate glassceramics," *Trans. Nonferrous Metals Soc. China* **24**(3), 729–735 (2014).
44. S. Yagi, "KTN crystals open up new possibilities and applications," *NTT Tech. Rev.* **7**(12), 1–5 (2009).
45. K. Nakamura, "Optical beam scanner using Kerr effect and space-chargecontrolled electrical conduction in $KTa_{1-x}Nb_xO_3$ crystal," *NTT Tech. Rev.* **5**(9), 1–8 (2007).
46. P. Yeh and A. Yariv, *Optical Waves in Crystals*, Wiley Series in Pure and Applied Optics, pp. 256–269, Wiley-Interscience, New York (1984).
47. J. F. Nye, *Physical Properties of Crystals: Their Representation by Tensors and Matrices*, pp. 254–257, Oxford University Press, Oxford (1957).
48. T. Imai et al., "Crystal growth and electro-optic properties of $KTa_{1-x}Nb_xO_3$," *NTT Techn. Rev.* **5**(9), 1–8 (2007).
49. H. Kogelnik, "Coupled wave theory for thick Hologram gratings," *Bell Syst. Tech. J.* **48**(9), 2909–2947 (1969).
50. I. V. Ciapurin, L. B. Glebov, and V. I. Smirnov, "Modeling of Gaussian beam diffraction on volume Bragg gratings in PTR glass," *Proc. SPIE* **5742**, 183–194 (2005).
51. L. Glebov, "Fluorinated silicate glass for conventional and holographic optical elements," *Proc. SPIE* **6545**, 654507 (2007).
52. L. Glebov, "Volume Bragg gratings in PTR glass—new optical elements for laser design," in *23rd Adv. Solid-State Photonics (ASSP) Topical Meeting*, ASSP Technical Digest, Paper Code MD1, Nara, Japan (2008).
53. T. Dorschner, "Raytheon steered agile beams," STAB, Final report, AFRL-SN-WP-TR-2004-1078, DTIC AD # is: ADB 302140 (2005).
54. M. Gottlieb, C. Irland, and J. Ley, *Electro-Optical and Acousto-Optis Scanning and Deflection*, Marcel Dekker, Inc., New York (1983).
55. "Acousto-optical beam steering study," Harris Corporation, RL-TR-91-121, 1994, https://apps.dtic.mil/dtic/tr/fulltext/u2/b191869.pdf (accessed 26 May 2029).
56. M. J. Escuti and W. M. Jones, "Polarization independent switching with high contrast from a liquid crystal polarization grating," *SID Symp. Dig.* **37**, 1443–1446 (2006).
57. M. J. Escuti and W. M. Jones, "A polarization-independent liquid crystal spatial light modulator," *Proc. SPIE* **6332**, 63320M (2006).
58. S. Serati, Private Communication, Boulder Nonlinear Systems (2019).
59. N. Tabiryan, Private Communication, BeamCo (2019).
60. T. Todorov, N. Tomova, and L. Nikolova, "High-sensitivity material with reversible photo-induced anisotropy," *Opt. Commun.* **47**, 123–126 (1983).
61. M. Attia and J. M. C. Jonathan, "Anisotropic gratings recorded from two circularly polarized coherent waves," *Opt. Commun.* **47**, 85–90 (1983).
62. B. Y. Zeldovich and N. V. Tabirian, "Devices for displaying visual information," Invention Disclosure, School of Optics/CREOL (2000).
63. H. Sarkissian et al., "Periodically aligned liquid crystal: potential application for projection displays and stability of liquid crystal configuration," in *Opt. Southeast; Conf. Program*, Orlando, Florida, PSE 02 (2003).
64. G. P. Crawford, J. N. Eakin, and M. D. Radcliffe, "Alignment of liquid crystals," US Patent Application 10/748,562 (2003).
65. J. Eakin et al., "Zero voltage Freedericksz transition in periodically aligned liquid crystals," *Appl. Phys. Lett.* **85**, 1671–1673 (2004).
66. G. Crawford et al., "Liquid-crystal diffraction gratings using polarization holography alignment techniques," *J. Appl. Phys.* **98**, 123102 (2005).
67. M. J. Escuti et al., "Polarization gratings in mesogenic films," PTO Patent Application PCT/IB2006/050615 (2005).
68. H. Sarkissian et al., "Polarization-controlled switching between diffraction orders in transverse-periodically aligned nematic liquid crystals," *Opt. Lett.* **31**(15), 2248–2250 (2006).
69. C. Provenzano, G. Cipparrone, and A. Mazzulla, "Photopolarimeter based on two gratings recorded in thin organic films," *Appl. Opt.* **45**, 3929–3934 (2006).
70. S. R. Nersisyan et al., "Optical axis gratings in liquid crystals and their use for polarization insensitive optical switching," *J. Nonlinear Opt. Phys. Mater.* **18**(1), 1–47 (2009).
71. S. R. Nersisyan et al., "The principles of laser beam control with polarization gratings introduced as diffractive waveplates," *Proc. SPIE* **7775**, 77750U (2010).
72. N. Tabiryan et al., "4G optics: new technology extends limits to the extremes," in *Photonics Spectra*, pp. 46–50 (2017).
73. J. Kim et al., "Wide-angle nonmechanical beam-steering using thin liquid crystal polarization gratings," *Proc. SPIE* **7093**, 709302 (2008).
74. J. Kim et al., "Efficient, wide-angle, nonmechanical beam steering via polarization gratings," *Appl. Opt.* **50**(17), 2636–2639 (2011).
75. J. Kim et al., "Demonstration of large-angle nonmechanical laser beam steering based on liquid crystal polymer polarization gratings," *Proc. SPIE* **8052**, 80520T (2011).
76. J. Kim et al., "Nonmechanical laser beam steering based on polymer polarization gratings: design optimization and demonstration," *J. Lightwave Technol.* **33**(10), 2068–2077 (2015).
77. H. Chen et al., "Beam steering for virtual/augmented reality displays with a cycloidal diffractive wave plate," *Opt. Express* **24**(7), 7287–7298 (2016).
78. T. Zhan et al., "Pancharatnam-Berry optical elements for head-up and near-eye displays," *J. Opt. Soc. Am. B* **36**(5), D52–D65 (2019).
79. M. J. Escuti et al., "Beam steering devices including stacked liquid crystal polarization gratings and related methods of operation," Provisional US Patent Application 61/230,227 (2009).
80. L. Shi, P. F. McManamon, and P. J. Bos, "Liquid crystal optical phase plate with a variable in-plane gradient," *J. Appl. Phys.* **104**, 033109 (2008).
81. P. F. McManamon and E. A. Watson, "Design of optical phased array beam steering with limited dispersion," in *Aerosp. Conf. Proc.*, IEEE (2001).
82. P. F. McManamon and E. A. Watson, "Nonmechanical beam steering for passive sensors," *Proc. SPIE* **4369**, 140–148 (2001).
83. E. A. Watson et al., "Application of dynamic gratings to broad spectral band beam steering," *Proc. SPIE* **2120**, 178–185 (1994).
84. V. G. Dominic, A. J. Carney, and E. A. Watson, "Measurement and modeling of the angular dispersion in liquid crystal broadband beam steering devices," *Opt. Eng.* **35**(12), 3371–3379 (1996).
85. G. M. Morris, "Diffraction theory for an achromatic Fourier transformation," *Appl. Opt.* **20**(11), 2017–2025 (1981).

Paul F. McManamon is president of Exciting Technology and Technical Director LOCI, University of Dayton. He chaired the National Academy of Sciences Study Laser Radar, (2014), and was cochair of "Optics and Photonics, Essential Technologies for Our Nation." He is a fellow of SPIE, IEEE, OSA, AFRL, DEPs, MSS, and AIAA. He was president of SPIE in 2006. He was chief scientist for the AFRL sensors directorate. He received his Meritorious Presidential Rank Award in 2006

Abtin Ataei: Biography is not available.